ESR modes in a Strong-Leg Ladder in the Tomonaga-Luttinger Liquid Phase

M. Ozerov,[1,*] M. Maksymenko,[2,3,4] J. Wosnitza,[1,5] A. Honecker,[6,7] C. P. Landee,[8]
M. M. Turnbull,[9] S. C. Furuya,[10] T. Giamarchi,[10] and S. A. Zvyagin[1]

[1]*Dresden High Magnetic Field Laboratory (HLD-EMFL), Helmholtz-Zentrum Dresden-Rossendorf, D-01328 Dresden, Germany*
[2]*Max-Planck-Institut für Physik komplexer Systeme, D-01187 Dresden, Germany*
[3]*Institute for Condensed Matter Physics, National Academy of Sciences of Ukraine, L'viv-79011, Ukraine*
[4]*Department of Condensed Matter Physics, Weizmann Institute of Science, Rehovot 76100, Israel*
[5]*Institut für Festkörperphysik, TU Dresden, D-01062 Dresden, Germany*
[6]*Institut für Theoretische Physik, Georg-August-Universität Göttingen, D-37077 Göttingen, Germany*
[7]*Laboratoire de Physique Théorique et Modélisation, CNRS UMR 8089, Université de Cergy-Pontoise, F-95302 Cergy-Pontoise Cedex, France*
[8]*Dept. of Physics and Carlson School of Chemistry, Clark University, Worcester, MA 01060, USA*
[9]*Carlson School of Chemistry and Biochemistry, Clark University, Worcester, MA 01610, USA*
[10]*Dept. of Quantum Matter Physics, University of Geneva, CH-1211 Geneva, Switzerland*

(Dated: February 21, 2015, revised September 7, 2015)

Magnetic excitations in the strong-leg quantum spin ladder compound $(C_7H_{10}N)_2CuBr_4$ (known as DIMPY) in the field-induced Tomonaga-Luttinger spin liquid phase are studied by means of high-field electron spin resonance (ESR) spectroscopy. The presence of a gapped ESR mode with unusual non-linear frequency-field dependence is revealed experimentally. Using a combination of analytic and exact diagonalization methods, we compute the dynamical structure factor and identify this mode with longitudinal excitations in the antisymmetric channel. We argue that these excitations constitute a fingerprint of the spin dynamics in a strong-leg spin-1/2 Heisenberg antiferromagnetic ladder and owe their ESR observability to the uniform Dzyaloshinskii-Moriya interaction.

PACS numbers: 75.40.Gb, 76.30.-v, 75.10.Jm

The investigation of spin systems where quantum effects play a dominant role has become a very active branch of quantum many-body physics. Although the spin Hamiltonian describing quantum magnets is quite simple and often very well controlled [1], the interplay of all spin degrees of freedom can be very complex, leading to a large diversity of phases ranging from long-range magnetic order to spin liquids of various types [2]. In addition, the ground state can possess not only local types of order but also more complex and subtle non-local topological orders [3, 4]. Understanding such behavior is thus a frontier of fundamental knowledge, providing, on the other hand, a potential means for quantum computation [5] or quantum simulators of some itinerant problems [6, 7].

Due to enhanced quantum effects, one- and quasi-one-dimensional (1D) spin systems, such as spin chains and ladders, are of particular interest [8]. In these systems, interactions between excitations can play a very important role, giving rise to exotic states [9], including quasi-long-range order, known as Tomonaga-Luttinger liquids (TLL), or phases where correlations between magnetic excitations are of short range (e.g., in the case of Haldane spin-1 chains [3]).

Recent progress in material science makes it possible to synthesize new materials with exchange parameters permitting the manipulation of the ground states by accessible magnetic fields, with drastic effects on the physical properties. This, and the progress in both analytical and numerical techniques provide access to a host of novel physics, allowing, e.g., the observation of the Bose-Einstein condensation of magnons [6, 10], the quantitative test for TLL predictions [11, 12], the observation of fractionalization of spin excitations [13, 14], spinon attraction [15], and remarkable effects of disorder [16–18].

Even very tiny anisotropies can play an important role, reducing local symmetries and drastically affecting the low-energy spin dynamics. Electron spin resonance (ESR) spectroscopy has proven to be one of the most sensitive tools to probe such interactions and effects in exchange-coupled spin systems [19]. One remarkable advantage of this technique is that ESR allows experiments in very high magnetic fields, far beyond the superconducting magnet limit [20–23]. Theoretical studies of predicted ESR parameters are available for spin chains and ladders [24–29], and have been applied with good success to, e.g., spin chains [30–32] and strong-rung ladders [33, 34]. However, relatively little is known about the spin dynamics in strong-leg ladder systems, which can be very different from that in spin chains and strong-rung ladders in terms of the spinon interactions.

In this work, we report on high-field ESR studies of the spin ladder $(C_7H_{10}N)_2CuBr_4$ [bis(2,3-dimethylpyridinium) tetrabromocuprate(II) or (2,3-dmpyH)$_2$-$CuBr_4$, abbreviated as DIMPY], currently known as the best realization of a strong-leg spin-1/2 Heisenberg antiferromagnetic ladder [35] with moderate exchange coupling constants. We reveal experimentally

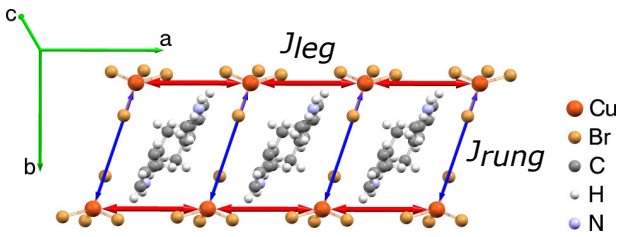

FIG. 1. (color online) Schematic view of the crystal structure of DIMPY [35]. The copper (Cu) ions form a ladder-like structure with the dominant exchange couplings indicated in the figure.

the presence of a novel ESR excitation mode in the TLL phase that is absent in a strong-rung ladder and was not observed in previous ESR work on DIMPY either [36]. We describe the unusual excitation spectrum of DIMPY, using a combination of analytic techniques and exact-diagonalization (ED) methods. We demonstrate that the appearance and magnetic-field dependence of parameters of the new mode can be understood by taking into account the dynamic spin-spin correlation function for the strong-leg spin-1/2 Heisenberg antiferromagnetic ladder model, thus providing important information on the spin excitations as well as the anisotropy of magnetic interactions in this system.

DIMPY crystallizes in a monoclinic lattice with space group P2(1)/n and lattice constants $a = 7.504\mathring{A}$, $b = 31.61\mathring{A}$, $c = 8.202\mathring{A}$, $\beta = 98.98^\circ$ (number of formula units per unit cell $Z = 4$) [35] with $S = 1/2$ Cu^{2+} ions arranged in a ladder-like structure (Fig. 1). Each unit cell contains two rungs, each from a different symmetry-equivalent ladder, running parallel to the a axis. The spin Hamiltonian of DIMPY can be written as

$$\mathcal{H} = J_{\rm leg} \sum_{\langle l,j \rangle} \mathbf{S}_{l,j} \cdot \mathbf{S}_{l+1,j} + J_{\rm rung} \sum_{\langle l \rangle} \mathbf{S}_{l,1} \cdot \mathbf{S}_{l,2} - g\mu_B H \sum_{l,j} S^z_{l,j} + \mathcal{H}_\delta, \quad (1)$$

where $J_{\rm leg}$ and $J_{\rm rung}$ are exchange coupling constants along the legs and rungs, respectively, $\mathbf{S}_{l,j}$ are the spin operators on site l of the leg $j = 1, 2$ of the ladder, $g\mu_B H$ is the Zeeman term (g is the g factor, μ_B is the Bohr magneton, H is the applied magnetic field). The fourth term represents various possible, usually small, anisotropic contributions. Exchange constants along the rungs and legs of the ladder have been determined by use of inelastic neutron scattering (INS) as $J_{\rm rung}/k_B \approx 9.5$ K and $J_{\rm leg}/k_B \approx 16.5$ K, respectively ($J_{\rm leg}/J_{\rm rung} \sim 1.73$) [37]. The ladders are coupled via very weak exchange interactions, $J'/k_B \lesssim 5-7$ mK [35–37], resulting in a transition into a field-induced magnetically ordered phase at temperatures below ~ 0.35 K [38].

In a strong-leg ladder, the transverse interchain interaction couples two spin chains. As a result, two spinons are confined to magnons, opening a spin gap in the excitation spectrum. In the presence of a magnetic field the gap in DIMPY closes at a critical field $H_{c1} = 2.8$ T, where the system undergoes a transition into the gapless TLL phase [39]. Above $H_{c2} = 29$ T, the system is in the magnetically saturated spin-polarized phase [40]. Inelastic neutron scattering experiments revealed the presence of several gapless continua as well as a number of gapped excitations in DIMPY [37, 41, 42]; some of the excitations have been interpreted theoretically. Investigating the field-induced evolution of the magnetic excitation spectrum of a strong-leg ladder in the TLL state is of particular interest, so far not covered in detail by theory and experiments. Such a study would allow to obtain a better understanding of peculiarities of the spin dynamics in a strong-leg ladder in the TLL phase, which is, as shown below, rather different from that known for quantum spin-1/2 chains and strong-leg ladders.

ESR experiments were performed at the Dresden High Magnetic Field Laboratory (Hochfeld Magnetlabor-Dresden), using transmission-type ESR spectrometers (similar to that described in Ref. [43]) equipped with 16 T superconducting and 50 T pulsed-field [44] magnets. VDI modular transmitters (product of Virginia Diodes Inc., USA) and backward-wave oscillators (PO Istok, Russia) were employed as sub-mm radiation sources. High-quality single-crystal samples of DIMPY with typical sizes of $2 \times 1 \times 1$ mm^3 were used in our experiments. The magnetic field was applied along the b axis. In our experiments 2,2-diphenyl-1-picrylhydrazyl (DPPH) with $g = 2.0036$ was used a standard ESR marker.

A single resonance line (Mode A, Fig. 2) was observed at temperatures above ~ 4 K. At lower temperatures, the ESR spectrum undergoes remarkable changes. In addition to Mode A we detected a relatively broad resonance absorption line (Mode B, Fig. 2). With decreasing temperature, Mode B becomes more intensive and narrower, shifting towards higher fields. Corresponding examples of the ESR spectra as well as the dependences of ESR linewidth (Mode B) on temperature and magnetic field are shown in Fig. 2 and Fig. 3, respectively.

The frequency-field diagram of the magnetic excitations in DIMPY is shown in Fig. 4. Mode A (white boxes in Fig. 4) can be described using the equation $h\nu = g_b\mu_B H$, where h is the Planck's constant, ν is the excitation frequency, and $g_b = 2.23$. Mode B (white circles in Fig. 4) has a more complex behavior: this mode is gapped for all fields and has a non-linear frequency-field dependence. From the extrapolation of the frequency-field dependence to zero field, the energy gap, $\Delta \sim 350$ GHz, can be estimated. This value agrees well with the size of the gap between the spin-singlet ground and first-excited triplet states observed by means of INS in zero magnetic field at $k = 0$ [41, 42], where the system is in the gapped

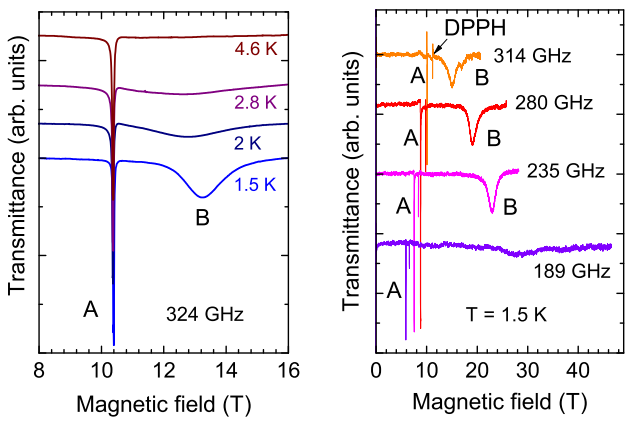

FIG. 2. (color online) Left panel: Examples of ESR spectra obtained at a frequency of 324 GHz at 1.5, 2, 2.8, and 4.6 K. Right panel: Examples of pulsed-field ESR spectra obtained at the frequencies 189, 235, 280, and 314.4 GHz ($T = 1.5$ K).

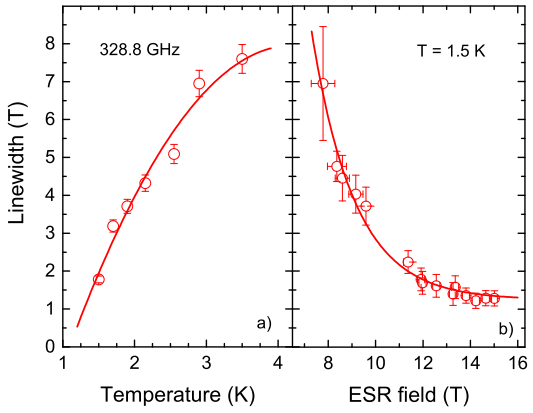

FIG. 3. (color online) (a) Temperature dependence of the linewidth of Mode B at a frequency of 328.8 GHz. (b) Linewidth of Mode B for different values of resonance fields ($T = 1.5$ K). Lines are guides to the eye.

spin-liquid state.

It is worth mentioning that the ESR excitation spectrum in DIMPY is very different from that in the strong-rung spin ladder BPCB [34], where only one gapless mode was observed in the TLL phase. The comparison of our ESR data with results of INS studies and ED calculations for DIMPY in the TLL regime [41] strongly suggests that the observed ESR Mode A corresponds to magnetic excitations in the $S_0^{\pm}$ channel, while Mode B corresponds to ESR excitations in the channel S_π^{zz}, which are nominally forbidden in the purely isotropic case. To demonstrate that S_π^{zz} indeed gives rise to Mode B, we calculated the field dependence of the dynamical structure factor employing ED of the model (1), where the anisotropic contribution $\mathcal{H}_\delta$ has been omitted. We used the parameters $J_{\rm leg}/J_{\rm rung} = 1.73$, $J_{\rm rung} = 9.51$ K, and $g = 2.23$ as determined above from the frequency-field dependence of Mode A [46]. The transverse dynamical structure factor $S_0^{\pm}$ in the symmetric channel of the legs and the longitudinal dynamical structure factor S_π^{zz} in the antisymmetric channel are calculated for finite systems of up to 64 sites using the expression

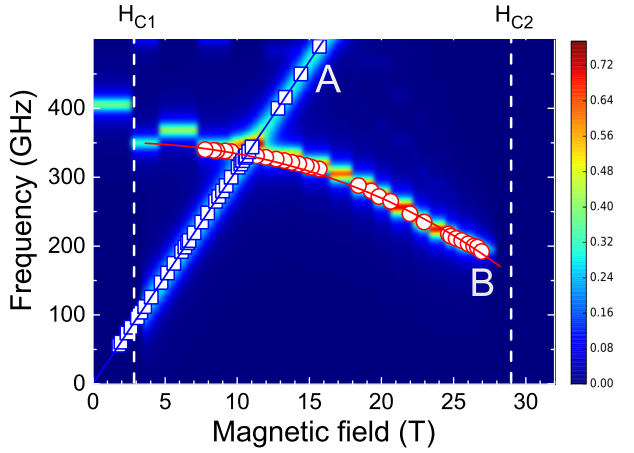

FIG. 4. (color online) The frequency-field diagram of magnetic excitations in DIMPY. Data of the structure factors S_π^{zz} and $S_0^{\pm}$ obtained by use of exact-diagonalization calculations for chains from $N = 32$ to $N = 64$ sites are given in bright colors [45]. Blue and red solid lines are guides to the eye. First and second critical fields are denoted by vertical dashed lines.

$$S^{\alpha\beta}_{k_\perp}(\omega) = \frac{1}{\pi}\sum_n \mathrm{Im}\,\frac{\langle 0|S^\alpha_{k_\perp}|n\rangle\,\langle n|S^\beta_{k_\perp}|0\rangle}{\omega - (\epsilon_n - \epsilon_0 + i\,\eta)}\,, \qquad (2)$$

for $T = 0$, where $|n\rangle$ are the eigenstates with energy ϵ_n ($|0\rangle$ is the ground state). η is a Lorentzian broadening that we set to $\eta = 0.05\,J_{\rm rung}$. The Fourier-transformed spin operators are given by

$$S^\alpha_{k_\perp} = \frac{1}{\sqrt{N}}\sum_{l,j}\exp(i\,k_\perp\,j)\,S^\alpha_{l,j}\,. \qquad (3)$$

Thus, $k_\perp$ is the momentum perpendicular to the ladder, while we have assumed zero momentum along the ladder direction, as is common for ESR.

We exploit the conservation of total S^z of the model (1). When the dimension of the subspace is sufficiently small, we use full diagonalization to evaluate (2) while for bigger dimensions we use first the Lanczos algorithm [47, 48] to find the ground state $|0\rangle$ and then a continued-fraction expansion [48–50] to obtain the spectral function (2).

Our ED results for the zero-temperature dynamical structure factors $S_0^{\pm}$ and S_π^{zz} are shown as intensity plots

in Fig. 4. Finite-size effects are strongest for low magnetic fields where they may amount to errors of up to 50 GHz for Mode B [45]. For magnetic fields $H > 12.5$ T, the main finite-size effects are the steps observed in "line" B and thus one may estimate them to not exceed 10 GHz here. The agreement of the position of the intensity maxima for $H \gtrsim 7$ T with the experimental ESR and INS [41] data is excellent, including not only the downward slope, but also the curvature of Mode B. We note further that application of ED to finite temperature [45] also reproduces the qualitative trends observed in Fig. 2 and Fig. 3 (a), in particular a substantial thermal broadening of Mode B.

As mentioned, ESR transitions corresponding to Mode B are nominally forbidden in the purely isotropic case. On the other hand, Fig. 1 shows that there is no inversion center on bonds along the ladder legs in the crystal structure of DIMPY and successive tetrabromocuprate units are related by unit cell translations [35]. This allows for the presence of a uniform Dzyaloshinskii-Moriya (DM) interaction along the legs of the form $\sum_l \sum_{j=1,2}(-1)^j \mathbf{D}\cdot(\mathbf{S}_{l,j}\times\mathbf{S}_{l+1,j})$. It is important to mention that the uniform DM interaction has been found responsible for a number of unusual effects, including, e.g., broadening of resonance line A, observed in DIMPY by means of low-frequency ESR spectroscopy [36] and the zero-field gap opening in the triangular-lattice antiferromagnet Cs_2CuCl_4 [51]. On the other hand, such a term accounts for the intensity of Mode B, that is directly proportional to the spin-spin correlations as discussed above [45]. In the low-field limit, Mode B can be described using the non-Abelian bosonization approach [52], where it is understood as a complex of two Majorana fermions [45]. The magnetic field couples symmetrically to the two legs of the ladder whereas the Majorana fermions are antisymmetric under the exchange $j = 1 \leftrightarrow j = 2$ of the two legs. Thus, to first approximation, Mode B is not affected by the applied field. This accounts for the almost flat behavior of Mode B observed in Fig. 4 up to about 15 T [45]. At higher magnetic fields, renormalization effects of these Majorana fermions are more important, resulting in the observed non-linear frequency-field dependence of Mode B.

Our observations of the S^{zz}_π mode can have broader impact in the context of the $SO(5)$ ladder model [53, 54]. In this model, the quantum phase transition driven by the chemical potential can be mapped to the field-induced phase transitions in the Heisenberg ladder. In that case, the gapless excitations in the TLL state of spin ladders (Mode A) are interpreted as massless t_{i+} bosons, while the gapped excitations (Mode B) correspond to massive $t_{i,0}$ bosons [54]. The former contribution is characteristic of the TLL state and is commonly found in spin-1/2 Heisenberg chains (and can be interpreted as originating from the Bose condensate of $\Delta S^z = 1$ magnons), while the latter have $\Delta S^z = 0$ magnons as their origin. The boson mass is determined by the Luttinger constant K (describing the nature of interactions between particles) and the velocity u; both parameters are field dependent [37]. The complex contributions of these two variables to the gapped excitation give a hint for understanding the non-linear dependence of Mode B in a magnetic field as observed in our experiments.

To summarize, the excitation spectrum in DIMPY, a spin-1/2 Heisenberg antiferromagnetic strong-leg ladder compound, was probed by means of high-field ESR in magnetic fields up to 50 T. Two ESR modes were observed. One of them has a linear frequency-field dependence, and corresponds to Zeeman-split massless $S^\pm_0$ excitations, commonly found in spin-1/2 Heisenberg chains and strong-rung ladders in the Tomonaga-Luttinger liquid regime. On the other hand, we show that a key property of the ESR spectrum in a spin-1/2 Heisenberg strong-leg ladder in the TLL phase is the presence of gapped S^{zz}_π excitations that derive from the gapped $\Delta S^z = 0$ boson. Good agreement between results of exact-diagonalization calculations and the experimental data was demonstrated.

This work was partially supported by the Helmholtz Gemeinschaft via the Virtual Institute "New states of matter and their excitations", Deutsche Forschungsgemeinschaft (DFG, Germany), Swiss SNF under Division II, and ERC synergy UQUAM project. We acknowledge the support of the HLD at HZDR, member of the European Magnetic Field Laboratory (EMFL).

Supplemental Material

UNIFORM DZYALOSHINSKII-MORIYA INTERACTION

Here, we show that a uniform Dzyaloshinskii-Moriya (DM) interaction along chains but staggered between chains can explain that the dynamical structure factor S^{zz}_π leads to an ESR signal and that there is, consequently, a nontrivial Mode B.

The symmetry of the crystal structure of DIMPY (Fig. 1 of the main manuscript) allows the occurrence of a uniform DM interaction along the leg, but staggered from leg to leg

$$\mathcal{H}_{\rm DM} = \sum_l \sum_{j=1,2} (-1)^j \mathbf{D}\cdot(\mathbf{S}_{l,j}\times\mathbf{S}_{l+1,j}), \qquad (4)$$

that corresponds to the term $\mathcal{H}_\delta$ of the Hamiltonian (1) in the main text. We choose coordinates in spin space such that the vector $\mathbf{D}$ points in the y direction, $\mathbf{D} = D\hat{y}$, where $\hat{y}$ is the unit vector along the y axis.

Since the DM interaction is very small, it hardly affects most physical quantities. One noteworthy exception is the selection rule of ESR excitations. The mode allowed

in the ESR spectrum strongly depends on weak perturbations breaking the spin-rotational symmetry. Normally, the ESR experiment measures $S_0^{\pm}$ at $k = 0$. The dynamical structure factor

$$S_0^{\pm}(\omega) = -\frac{1}{1-e^{-\omega/T}} \operatorname{Im} G^R_{S^+S^-}(\omega) \tag{5}$$

is proportional to the imaginary part of the retarded Green's function at $k = 0$,

$$G^R_{S^+S^-}(\omega) = -i\int_0^\infty dt e^{i\omega t}\langle[S^+(t), S^-(0)]\rangle, \tag{6}$$

where $S^+ = \sum_l \sum_{j=1,2} S^+_{l,j}$. Since the prefactor in Eq. (5) does not have special resonances in frequency, the ESR modes A and B mentioned in the main manuscript come from the frequency dependence of the retarded Green's function (6). In order to investigate the origin of these modes, we utilize the following *identity* (compare with the appendix of Ref. [55])

$$G^R_{S^+S^-}(\omega) = \frac{2\langle S^z\rangle}{\omega - g\mu_B H} - \frac{\langle[\mathcal{A}, S^-]\rangle}{(\omega - g\mu_B H)^2} + \frac{1}{(\omega - g\mu_B H)^2} G^R_{\mathcal{A}\mathcal{A}^\dagger}(\omega)\,, \tag{7}$$

where $\mathcal{A}$ is the operator $\mathcal{A} = [\mathcal{H}_{\rm DM}, S^+]$. According to the identity (7), in the absence of the DM interaction (i.e., $\mathcal{A} = 0$), one finds a single mode at $\omega = g\mu_B H$, which is Mode A. The ESR mode B is absent unless anisotropic interactions breaking the spin-rotational symmetry are present. The identity (7) also shows that Mode B comes from the last term, the retarded Green's function $G^R_{\mathcal{A}\mathcal{A}^\dagger}(\omega)$. The operator $\mathcal{A}$ is given by

$$\mathcal{A} = \sum_l \sum_{j=1,2} (-1)^j D(S^y_{l,j} S^x_{l+1,j} - S^x_{l,j} S^y_{l+1,j}). \tag{8}$$

The above formula is exact and valid for arbitrary magnetic field.

We can get an approximation valid for low energy, long wavelength by replacing $S^{x,y}_{l+1,j} \to S^{x,y}_{l,j}$. In that case Eq. (8) becomes $\mathcal{A} = -iD\sum_l \sum_{j=1,2}(-1)^j S^z_{l,j}$. and one obtains

$$S^{zz}_\pi \approx -D^{-2}\,(1-e^{-\omega/T})^{-1} \operatorname{Im} G^R_{\mathcal{A}\mathcal{A}^\dagger}(\omega) \tag{9}$$

Mode B is thus directly connected to the zz spin spin correlation function in the absence of DM interactions.

In order to complement the above description of Mode B we employ a bosonization approach dealing with the rung interaction, $J_{\rm rung}$, perturbatively. The bosonization provides a perfectly controllable treatment of the low-energy theory for $J_{\rm rung}/J_{\rm leg} \ll 1$. Although for DIMPY the ratio is too high to expect quantitative agreement we can expect a very good qualitative description.

The standard non-Abelian bosonization calculation leads to [56]

$$\mathcal{A} \approx \frac{D}{\pi\alpha}\int dx \sum_{j=1,2} (-1)^j [J^z_{jR}(x) - J^z_{jL}(x)], \tag{10}$$

where α is the short-distance cutoff. $J_{jR}(x)$ and $J_{jL}(x)$ are, respectively, the right-moving and the left-moving components of the $SU(2)$ current on the jth leg. Note that the spin $\mathbf{S}_{l,j}$ is written as $\mathbf{S}_{l,j} \approx \mathbf{J}_{jR}(x) + \mathbf{J}_{jL}(x) + (-1)^{l+j}\mathbf{N}(x)$, where $\mathbf{N}(x)$ is the Néel order parameter. According to Ref. [57], we can rewrite the operator (10) by using two Majorana fermions,

$$\mathcal{A} \approx \gamma D \int dx\,(\xi_R\rho_R - \xi_L\rho_L). \tag{11}$$

Here, γ is a non-universal constant. $\xi_{R(L)}$ and $\rho_{R(L)}$ are the right-moving (left-moving) component of the Majorana fermions ξ and ρ. The Majorana fermion ξ, when it is applied to the singlet ground state at zero magnetic field, generates a triplon with $S^z = 0$. Although Ref. [57] formulated the refermionized theory for the $H = 0$ case, one can easily extend it to the high-field case of our interest. At the level of the bosonized and refermionized theory, the Hamiltonian of the spin ladder at $H = 0$ is split into two parts: a symmetric and an antisymmetric part with respect to the permutation of the leg index $j = 1 \leftrightarrow j = 2$. The magnetic field affects the symmetric sector only and can induce a quantum phase transition from the gapped phase at low field into the field-induced Tomonaga-Luttinger liquid phase. Conversely the Majorana fermions ξ and ρ belong to the antisymmetric sector [57], are thus in first approximation unaffected by the magnetic field, and retain a gapful excitation spectrum. If we call Δ_0 the excitation gap of ξ at $k = \pi$, the other Majorana fermion ρ has a higher excitation gap $3\Delta_0$ at $k = 0$ [57]. Hence, the operator (11) generates multi-particle excitations whose excitation gap at $k = 0$ equals to $4\Delta_0$. For zero magnetic field the triplet gap Δ_0 is estimated from our exact diagonalization data as $\Delta_0 \approx 4.3$ K (see section below) leading to a value $4\Delta_0 \approx 17.2$ K ≈ 360 GHz of the resonance frequency of Mode B in good agreement with $\Delta \sim 350$ GHz obtained from the extrapolation of the frequency-field dependence of the Mode B to zero field (see Fig. 4 in the main text). At finite magnetic field the decoupling of the symmetric and antisymmetric mode would naively yield a field-independent frequency. However there are irrelevant operators that couple these two sectors. Although they do not change the asymptotic physics they can renormalize the value of the parameters, hence a field dependence of the resonance that must be computed numerically.

EXACT DIAGONALIZATION OF FINITE LADDERS

Zero temperature

The field dependence of the dynamical structure factors in the $S_0^{\pm}$ and S_π^{zz} channels at $k = 0$ along the legs has been computed at $T = 0$ using exact diagonalization (ED) of the model Hamiltonian [Eq. (1) in the main text] for finite systems of sizes up to 64 sites. For $N \leq 20$ and in the high S^z sectors we use full diagonalization, otherwise a combination of the Lanczos algorithm with a continued fraction expansion [47–50].

The action of the operators $S^{\pm}$ changes the quantum number S^z by ± 1, rendering the computation of $S_0^{\pm}$ more challenging than S_π^{zz}. Nevertheless, only a strong line at frequency $\omega = g\,\mu_B\,H$ has been observed in $S_0^{\pm}$ with an intensity subject to small finite-size effects. Since furthermore the mixing of the two channels depends on parameters like the length of the DM vector D that are not really known, we manually added a line for $S_0^{\pm}$ with a suitable intensity in Fig. 4 of the main text.

We now focus on the channel S_π^{zz} since this exhibits a more complex behavior. For completeness, we start with the case of zero magnetic field in the top panel of Fig. 5 even if this has been investigated previously [15, 37, 41, 42]. The low-field region is particularly challenging for ED since on the one hand the numerical effort is maximal and on the other hand finite-size effects are largest, compare the position of the main peak in Fig. 5. Nevertheless, the inset of the top panel of Fig. 5 demonstrates that the peak position $\omega_{\rm peak}$ at $H = 0$ can be extrapolated to $\Delta \approx 360$ GHz in the thermodynamic limit $N \to \infty$. Note that a similar extrapolation can also be performed for the spin gap Δ_0: a fit with an exponential function gives rise to $\Delta_0 \approx 4.3$ K ≈ 90 GHz, corresponding to a first critical field $H_{c1} \approx 2.9$ T. As a consistency check of these two independent extrapolations, we mention that the ratio Δ/Δ_0 reproduces the field-theory prediction $\Delta/\Delta_0 = 4$ very accurately.

The higher magnetic fields that are our main concern are more favorable for two reasons. Firstly, exact diagonalization is performed for lower particle numbers and one can reach bigger system sizes. In addition, finite-size effects become less important. The case $g\mu_B H = 3J_{\rm rung}$ shown in the middle panel of Fig. 5 demonstrates a well-behaved case. In this case the ground state is in the sector $S^z = N/4$ (half of the saturation magnetization) for all considered systems and finite-size effects are virtually absent, as is demonstrated by the lines for all system sizes falling on top of each other in the middle panel of Fig. 5.

Finally, the bottom panel of Fig. 5 illustrates the more typical behavior with the case $g\mu_B H = 4J_{\rm rung}$. In this case, the ground state is in the sector $S^z = 3\,N/8$ for those N that are divisible by 8, i.e., $N = 24$, 32, 40, and 48 in the figure. For these system sizes, again no finite-size effects are observable. On the other hand, if N

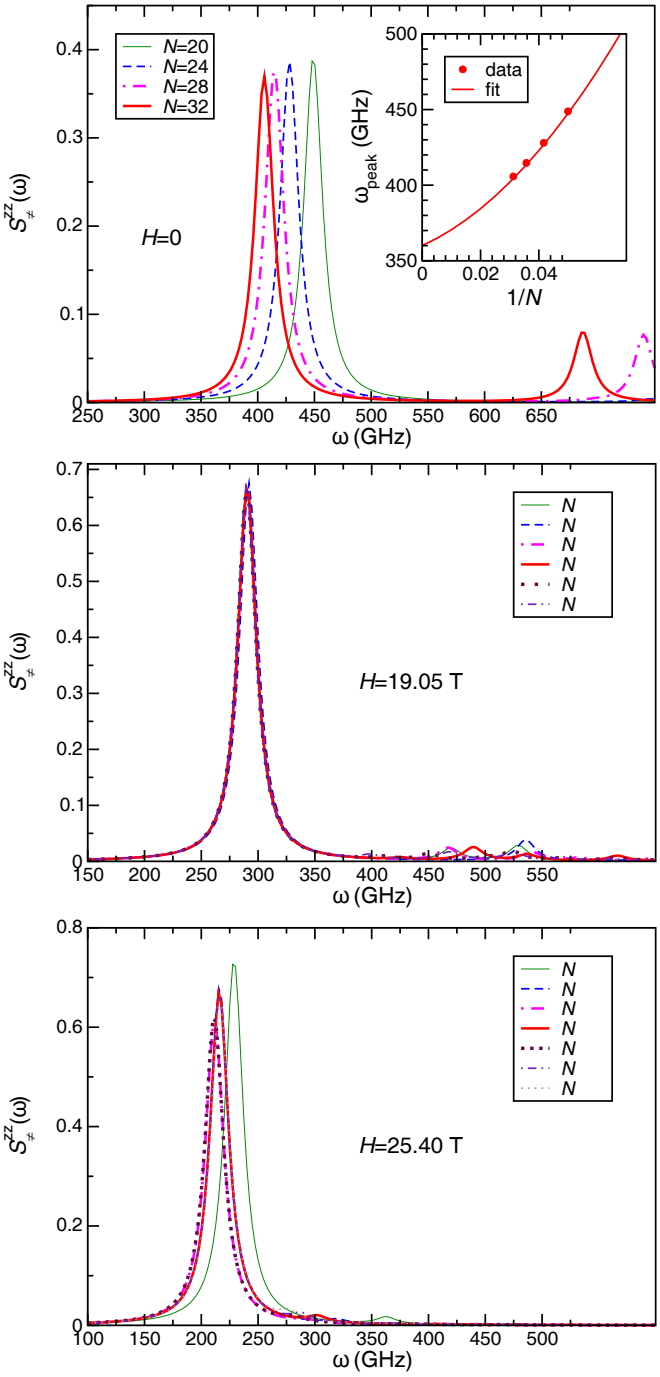

FIG. 5. (color online) Finite-size dependence of the S_π^{zz} structure factor at the temperature $T = 0$ and magnetic fields $H = 0$ (top panel), $H = 19.05$ T (middle panel), and $H = 25.40$ T (bottom panel). A Lorentzian broadening of $\eta = 0.05\,J_{\rm rung} \approx 10$ GHz is applied. The inset of the top panel shows a finite-size extrapolation of the frequency of the peak $\omega_{\rm peak}$ using a quadratic fit in the inverse system size $1/N$.

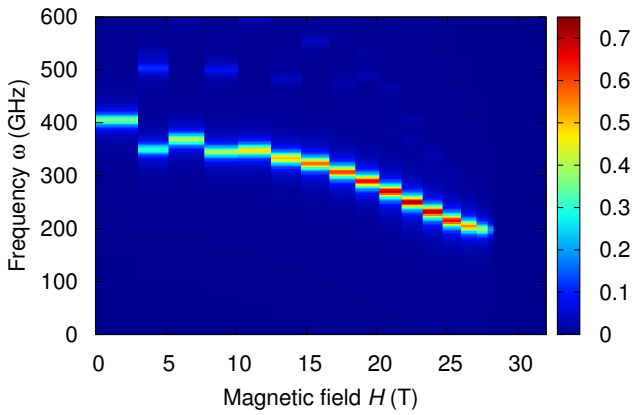

FIG. 6. (color online) Frequency-field diagram of a finite ladder of $N = 32$ sites. The shading encodes the value of the structure factor S^{zz}_{π}.

is not divisible by 8, $S^z = 3\,N/8$ cannot be realized and the corresponding system sizes ($N = 20$, 28, and 36 in the figure) scatter a bit around the thermodynamic limit. For systems with $N \geq 32$ spins and in the high-field region, these finite-size shifts of the main line should not exceed 10 GHz. Above this main peak there is always a bit of spectral density corresponding to continua of excitations. Since these continua need to be approximated by a finite number of peaks for fixed N, one naturally observes that these continua are more strongly affected by finite-size effects.

Figure 6 shows the field dependence of S^{zz}_{π} for a fixed system size of $N = 32$ spins. The jumps of the "line" in the low-field region in Fig. 6 reflect again the finite-size effects discussed above, but for higher magnetic fields the main effect is that only discrete values of S^z/N are realized for a fixed system size. Fig. 4 of the main text is based on a composite of the largest available system sizes and coincides with the present Fig. 6 in the region $H < 13.65$ T (in Fig. 4 of the main text we have used $N = 36$ for $H > 13.65$ T, $N = 40$ for $H > 18.86$ T, $N = 48$ for $H > 23.17$ T, and $N = 64$ for $H > 26.03$ T). Note that $S^{zz}_{\pi}(\omega) \equiv 0$ in the sector with $S^z = N/2 - 1$ just before saturation. In the case $N = 32$ shown in the present Fig. 6 this implies a vanishing signal already at a field of ≈ 27.9 T, i.e., below the saturation field $H_{c2} = 29$ T. In the case of Fig. 4 of the main text we have used data for $N = 64$ spins just below saturation. Accordingly, this apparent saturation field is closer to the true saturation field, namely at ≈ 28.2 T.

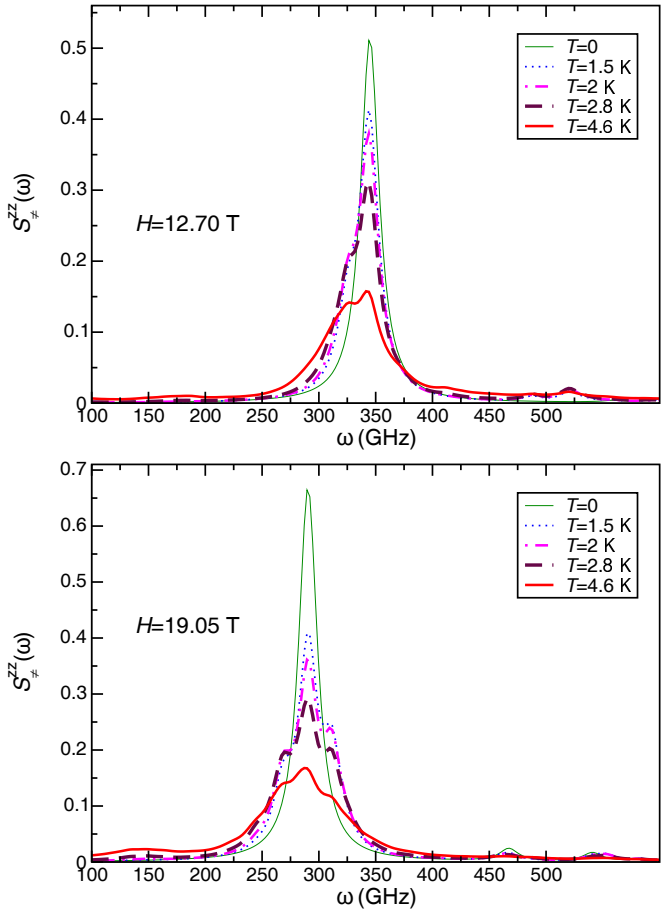

FIG. 7. (color online) Temperature dependence of the S^{zz}_{π} structure factor at a magnetic fields $H = 12.70$ T (upper panel) and $H = 19.05$ T (lower panel). The size of the system is fixed at $N = 28$ sites and a Lorentzian broadening of $\eta = 0.05\,J_{\rm rung} \approx 10$ GHz is applied.

Finite temperature

Finally, we take a brief look at $T > 0$. First, we need a generalization of Eq. (2) of the main text

$$S^{\alpha\alpha}_{k_\perp}(\omega) = \frac{1}{\pi}\sum_{n,m}\frac{e^{-\frac{\epsilon_m}{k_B\,T}}}{Z}\,\mathrm{Im}\,\frac{\left|\langle n|S^{\alpha}_{k_\perp}|m\rangle\right|^2}{\omega - (\epsilon_n - \epsilon_m + i\,\eta)}\,, \quad (12)$$

where $Z = \sum_m e^{-\epsilon_m/(k_B\,T)}$ is the partition function. Here we present ED results for $N = 28$ sites. In this case, we can no longer obtain the full spectrum, but we need to restrict the sums over m to low energies ϵ_m. After performing such a restriction, the spectral sum over n is again evaluated by a continued fraction expansion [48–50]. This approximation would break down at high temperatures, but is accurate for the region of interest, i.e., temperatures $k_B\,T < J_{\rm rung}/2$. Since we need to compute excited states with the Lanczos algorithm [47, 48], we have to work with smaller systems than for zero tem-

perature. At least 20 states have been retained for each sector with a given S^z and momentum $\vec{k}$.

Figure 7 presents results for two cases, namely $H = 2\,J_{\rm rung}/(g\,\mu_B) \approx 12.70$ T (upper panel) and $H = 3\,J_{\rm rung}/(g\,\mu_B) \approx 19.05$ T (lower panel). The $T = 0$ limit of the latter case has been presented before in the middle panel of Fig. 5 where finite-size effects were observed to be small. At finite T, finite-size effects are still visible as wiggles in the detailed lineshape. Still, Fig. 7 clearly demonstrates a substantial broadening and corresponding damping as temperature is raised to 4.6 K. This is in qualitative agreement with the experimental findings (left panel of Fig. 2 and 3(a) of the main text). At $H = 3\,J_{\rm rung}/(g\,\mu_B) \approx 19.05$ T there is no observable shift of the position of the line with temperature whereas for $H = 2\,J_{\rm rung}/(g\,\mu_B) \approx 12.70$ T one observes a shift of the center of mass of the line to lower frequency ω with rising temperature, at least for the $N = 28$ system shown in Fig. 7. Given the downward slope of Mode B with increasing magnetic field H, this translates to a shift of the mode to lower fields with rising temperature when one translates the present frequency scans at constant field to field scans at constant frequency. Thus, the shift observed in the upper panel of Fig. 7 is consistent with the shift of Mode B observed experimentally (left panel of Fig. 2 of the main text). Between $T = 0$ and 1.5 K there is generally a bit of broadening, but no significant shift of the main line, justifying the comparison of $T = 0$ computations with experiments performed at 1.5 K.

* Present Address: FELIX Laboratory, Radboud University, 6525 ED Nijmegen, The Netherlands

[1] A. Auerbach, *Interacting Electrons and Quantum Magnetism* (Springer, Berlin, 1998).
[2] L. Balents, Nature **464**, 199 (2010).
[3] F. D. M. Haldane, Phys. Rev. Lett. **50**, 1153 (1983).
[4] M. P. M. den Nijs, Phys. Rev. B. **23**, 6111 (1981).
[5] C. Nayak, S. Simon, A. Stern, M. Freedman, and S. Das Sarma, Rev. Mod. Phys. **80**, 1083 (2008).
[6] T. Giamarchi, C. Rüegg, and O. Tchernyshyov, Nature Physics **4**, 198 (2008).
[7] S. Ward, P. Bouillot, H. Ryll, K. Kiefer, K. W. Krämer, C. Rüegg, C. Kollath, and T. Giamarchi, J. Phys.: Condens. Matter **25**, 014004 (2013).
[8] E. Dagotto and T. M. Rice, Science **271**, 618 (1996).
[9] T. Giamarchi, *Quantum Physics in one Dimension*, International series of monographs on physics, Vol. 121 (Oxford University Press, Oxford, UK, 2004).
[10] V. Zapf, M. Jaime, and C. D. Batista, Rev. Mod. Phys. **86**, 563 (2014).
[11] M. Klanjšek, H. Mayaffre, C. Berthier, M. Horvatić, B. Chiari, O. Piovesana, P. Bouillot, C. Kollath, E. Orignac, R. Citro, and T. Giamarchi, Phys. Rev. Lett. **101**, 137207 (2008).
[12] K. Y. Povarov, D. Schmidiger, N. Reynolds, R. Bewley, and A. Zheludev, Phys. Rev. B **91**, 020406 (2015).
[13] B. Thielemann, C. Rüegg, H. M. Rønnow, A. M. Läuchli, J.-S. Caux, B. Normand, D. Biner, K. Krämer, H.-U. Güdel, J. Stahn, K. Habicht, K. Kiefer, M. Boehm, D. F. McMorrow, and J. Mesot, Phys. Rev. Lett. **102**, 107204 (2009).
[14] P. Bouillot, C. Kollath, A. M. Läuchli, M. Zvonarev, B. Thielemann, C. Rüegg, E. Orignac, R. Citro, M. Klanjšek, C. Berthier, M. Horvatić, and T. Giamarchi, Phys. Rev. B. **83**, 054407 (2011).
[15] D. Schmidiger, S. Mühlbauer, S. N. Gvasaliya, T. Yankova, and A. Zheludev, Phys. Rev. B **84**, 144421 (2011).
[16] T. Hong, A. Zheludev, H. Manaka, and L.-P. Regnault, Phys. Rev. B. **81**, 060410(R) (2010).
[17] A. Oosawa and H. Tanaka, Phys. Rev. B. **65**, 184437 (2002).
[18] R. Yu, L. Yin, N. S. Sullivan, J. S. Xia, C. Huan, A. Paduan-Filho, N. F. Oliveira Jr, S. Haas, A. Steppke, C. F. Miclea, F. Weickert, R. Movshovich, E.-D. Mun, B. L. Scott, V. S. Zapf, and T. Roscilde, Nature **489**, 379 (2012).
[19] A. Bencini and D. Gatteschi, *EPR of Exchange Coupled Systems* (Springer, Berlin, 1990).
[20] S. A. Zvyagin, M. Ozerov, E. Čižmár, D. Kamenskyi, S. Zherlitsyn, T. Herrmannsdörfer, J. Wosnitza, R. Wünsch, and W. Seidel, Rev. Sci. Instrum. **80**, 073102 (2009).
[21] S. A. Zvyagin, E. Čižmár, M. Ozerov, J. Wosnitza, R. Feyerherm, S. R. Manmana, and F. Mila, Phys. Rev. B. **83**, 060409(R) (2011).
[22] M. Ozerov, J. Romhanyi, M. Belesi, H. Berger, J. P. Ansermet, J. van den Brink, J. Wosnitza, S. A. Zvyagin, and I. Rousochatzakis, Phys. Rev. Lett. **113**, 157205 (2014).
[23] H. Nojiri, Y. Shimamoto, N. Miura, M. Hase, K. Uchinokura, H. Kojima, I. Tanaka, and Y. Shibuya, Phys. Rev. B. **57**, 10276 (1998).
[24] M. Oshikawa and I. Affleck, Phys. Rev. Lett. **79**, 2883 (1997).
[25] I. Affleck and M. Oshikawa, Phys. Rev. B **60**, 1038 (1999).
[26] I. Affleck and M. Oshikawa, Phys. Rev. B **62**, 9200 (2000).
[27] M. Brockmann, F. Göhmann, M. Karbach, A. Klümper, and A. Weiße, Phys. Rev. Lett. **107**, 017202 (2011).
[28] S. Furuya and M. Oshikawa, Phys. Rev. Lett. **109**, 247603 (2012).
[29] S. C. Furuya and M. Sato, J. Phys. Soc. Jpn. **84**, 033704 (2015).
[30] S. A. Zvyagin, A. K. Kolezhuk, J. Krzystek, and R. Feyerherm, Phys. Rev. Lett. **93**, 027201 (2004).
[31] S. A. Zvyagin, A. K. Kolezhuk, J. Krzystek, and R. Feyerherm, Phys. Rev. Lett. **95**, 017207 (2005).
[32] A. A. Validov, M. Ozerov, J. Wosnitza, S. A. Zvyagin, M. M. Turnbull, C. P. Landee, and G. B. Teitel'baum, J. Phys.: Condens. Matter **26**, 026003 (2014).
[33] S. C. Furuya, P. Bouillot, C. Kollath, M. Oshikawa, and T. Giamarchi, Phys. Rev. Lett. **108**, 037204 (2012).
[34] E. Čižmár, M. Ozerov, J. Wosnitza, B. Thielemann, K. W. Krämer, C. Rüegg, O. Piovesana, M. Klanjšek, M. Horvatić, C. Berthier, and S. A. Zvyagin, Phys. Rev. B. **82**, 054431 (2010).
[35] A. Shapiro, C. P. Landee, M. M. Turnbull, J. Jornet, M. Deumal, J. J. Novoa, M. A. Robb, and W. Lewis, J.

Am. Chem. Soc. **129**, 952 (2007).
[36] V. N. Glazkov, M. Fayzullin, Y. Krasnikova, G. Skoblin, D. Schmidiger, S. Mühlbauer, and A. Zheludev, Phys. Rev. B **92**, 184403 (2015).
[37] D. Schmidiger, P. Bouillot, S. Mühlbauer, S. Gvasaliya, C. Kollath, T. Giamarchi, and A. Zheludev, Phys. Rev. Lett. **108**, 167201 (2012).
[38] M. Jeong, H. Mayaffre, C. Berthier, D. Schmidiger, A. Zheludev, and M. Horvatić, Phys. Rev. Lett. **111**, 106404 (2013).
[39] T. Hong, A. Zheludev, H. Manaka, and L.-P. Regnault, Phys. Rev. B **81**, 060410 (2010).
[40] J. L. White, C. Lee, O. Gunaydin-Sen, L. C. Tung, H. M. Christen, Y. J. Wang, M. M. Turnbull, C. P. Landee, R. D. McDonald, S. A. Crooker, J. Singleton, M. H. Whangbo, and J. L. Musfeldt, Phys. Rev. B. **81**, 052407 (2010).
[41] D. Schmidiger, P. Bouillot, T. Guidi, R. Bewley, C. Kollath, T. Giamarchi, and A. Zheludev, Phys. Rev. Lett. **111**, 107202 (2013).
[42] D. Schmidiger, S. Mühlbauer, A. Zheludev, P. Bouillot, T. Giamarchi, C. Kollath, G. Ehlers, and A. M. Tsvelik, Phys. Rev. B. **88**, 094411 (2013).
[43] S. A. Zvyagin, J. Krzystek, P. H. M. van Loosdrecht, G. Dhalenne, and A. Revcolevschi, Physica B **346-347**, 1 (2004).
[44] M. Ozerov, "High-field electron spin resonance in low-dimensional spin systems," Ph.D. Thesis, TU Dresden (2011).
[45] For more details on the effect of the DM interaction, the non-Abelian bosonization analysis, and exact diagonalization compare the Supplemental Material.
[46] This yields $H_{c1} \approx 2.9$ T and a saturation field $H_{c2} \approx 28.32$ T, in good agreement with the experimental values $H_{c1} = 2.8$ T and $H_{c2} = 29.0$ T [40].
[47] C. Lanczos, J. Res. Nat. Bur. Stand. **45**, 255 (1950).
[48] E. Dagotto, Rev. Mod. Phys. **66**, 763 (1994).
[49] R. Haydock, V. Heine, and M. J. Kelly, J. Phys. C: Solid State Phys. **5**, 2845 (1972).
[50] E. R. Gagliano and C. A. Balseiro, Phys. Rev. Lett. **59**, 2999 (1987).
[51] K. Y. Povarov, A. I. Smirnov, O. A. Starykh, S. V. Petrov, and A. Y. Shapiro, Phys. Rev. Lett. **107**, 037204 (2011).
[52] D. G. Shelton, A. A. Nersesyan, and A. M. Tsvelik, Phys. Rev. B **53**, 8521 (1996).
[53] D. Scalapino, S.-C. Zhang, and W. Hanke, Phys. Rev. B **58**, 443 (1998).
[54] A. Furusaki and S. Zhang, Phys. Rev. B. **60**, 1175 (1999).
[55] M. Oshikawa and I. Affleck, Phys. Rev. B **65**, 134410 (2002).
[56] S. Gangadharaiah, J. Sun, and O. A. Starykh, Phys. Rev. B **78**, 054436 (2008).
[57] D. G. Shelton, A. A. Nersesyan, and A. M. Tsvelik, Phys. Rev. B **53**, 8521 (1996).